Particle Size Control and Self-Assembly Processes in Novel Colloids of Nanocrystalline Manganese Oxide

Stephanie L. Brock,[†] Maria Sanabria,[†] and Steven L. Suib*[,†,‡]

Department of Chemistry, University of Connecticut, U-60, 55 North Eagleville Rd., Storrs, Connecticut 06269-3060, and Department of Chemical Engineering and Institute of Materials Science, University of Connecticut, Storrs, Connecticut 06269

Volker Urban and Pappannan Thiyagarajan

Intense Pulsed Neutron Source Division, Argonne National Laboratory, 9700 South Cass Avenue, Argonne, Illinois 60439

Donald I. Potter

Department of Metallurgy and Materials Engineering, University of Connecticut, Storrs, Connecticut 06269-3136

Received: March 24, 1999; In Final Form: June 17, 1999

The synthesis of semiconducting nanocrystals of manganese oxide of controlled sizes and their manipulation to form ordered arrays is described. Nanocrystalline mixed-valent manganese oxides have been prepared as colloidal solutions via reduction of tetraalkylammonium (methyl, ethyl, propyl, and butyl) permanganate salts in aqueous solutions with 2-butanol and ethanol. Reduction with the poorly water miscible 2-butanol produces aqueous colloids for the methyl, ethyl, and propyl systems, whereas 2-butanol colloids are produced for the butyl system. The colloids are reddish-brown, have an average manganese oxidation state of 3.70−3.79, and have been prepared in manganese concentrations up to 0.57 M. The sols will gel upon aging, and the gel time depends on the cation, the amount of alcohol, the temperature, and the concentration of manganese. Small angle neutron scattering (SANS) data indicate that the particles are disklike in shape with radii in the range 20−80 Å and are largely unassociated in solution. Thin films produced from evaporation of the colloid or spreading of the gel onto glass slides demonstrate long-range order, yielding an X-ray diffraction (XRD) pattern consistent with a structure of CdI_2-type layers of manganese oxide with tetraalkylammonium cations and water molecules interspersed between the layers. The SANS and XRD evidence are consistent with a mechanism of self-assembly of unassociated layers upon concentration and evaporation. Consistent with a mechanism of quantum confinement, UV/visible spectroscopy of the colloids reveals two absorbances, one near 220 nm and the other in the range 290−310 nm, blue-shifted from the maxima observed for bulk manganese oxide (400 nm). When the samples are aged, these bands shift to the red. The growth of particles in solution with aging, indicated by the shifts in absorbance, has been confirmed by SANS experiments.

Introduction

Crystallites of nanometer dimensions demonstrate a host of unusual properties that set them apart from both extended and molecular materials. These properties are due to the electronic structure and the surface-to-volume ratio, both of which, in the nanometer regime, are strongly related to size.[1] Semiconductor nanocrystalline materials have been an area of intense investigation, and there has been much effort focused on the synthesis and properties of these materials including nanocrystals of silicon[2,3] and II−VI[4] and III−V[5] semiconductors. One particularly interesting area, in terms of variety of properties and applications, is the investigation of semiconductor metal oxide nanocrystals. Nanocrystalline oxides of Zn, V, Co, Ti, and Ce are of interest as catalysts and photocatalysts, battery materials, phosphors, and supports because of their high surface area coupled with size-dependent electronic and optoelectronic properties.[6] For device manufacture it is not sufficient to merely produce nanocrystals, and researchers have turned their attention to techniques for assembling nanocrystals into ordered three-dimensional arrays.[7]

Manganese oxides with mixed-valent manganese comprise a large class of semiconducting materials with unique properties.[8] They find application as cathodes in lithium ion batteries,[9] are good oxidation catalysts,[10] and recently have been found to exhibit giant or colossal magnetoresistance.[11] Nanocrystalline manganese oxides may produce a new set of properties complementary to those in the bulk, improving or augmenting the applications for manganese oxide. While bulk preparations have been extensively explored,[12−21] there have been few reported preparations and/or investigations of manganese oxide nanoparticles.[22−27] Stable nanoparticles of manganese oxide can be difficult to prepare because of the strong tendency of manganese oxide to precipitate or coagulate during the synthesis. Unlike conventional semiconducting materials such as CdS or

* To whom correspondence should be addressed.
[†] Department of Chemistry
[‡] Department of Chemical Engineering and Institute of Materials Science.

10.1021/jp991009u CCC: $18.00
Published on Web 08/12/1999

GaAs, many manganese oxides are negatively charged and ionically associated with cations including alkali metal cations, alkaline earth metal cations, and protons. It is the close association of these cations that balances the charge of the manganese oxide units, permitting condensation into larger particles. Altering this ionic interaction through the incorporation of large, less electropositive organic cations may prove to be a fruitful way to control nucleation and condensation, permitting the formation of new manganese oxide structures and nanocrystalline manganese oxide materials.

We have undertaken a systematic study of the effects of organic cations on the synthesis of manganese oxides. Although extensively studied in other transition metal oxide systems,[28−35] previous attempts to incorporate organic cations into the synthesis matrix for manganese oxides have been largely unsuccessful because of competition with inorganic cations in the synthesis matrix, which induces rapid precipitation or coagulation.[36,37] A notable exception has been the recent preparation of manganese oxide mesoporous materials from surfactants.[38] We have developed a new synthetic route to manganese oxides that precludes the presence of inorganic cations. Here, we report the successful preparation of stable colloids of lamellar manganese oxide from reduction of tetraalkylammonium (tetramethylammonium, tetraethylammonium, tetrapropylammonium, and tetrabutylammonium) permanganate precursors. These materials are unique with respect to any nanocluster manganese oxide materials prepared to date in that they can be prepared at very high concentrations, the particle size can be controlled, and they are crystalline and can be organized into ordered arrays. As such, they open the door for the rational orchestration of nanoparticles to produce nanostructured materials with designed structure−property relationships. The structure, particle size, and optical properties of these colloids, as well as their self-assembly into layered phases incorporating tetraalkylammonium cations, will be described.

Experimental Procedures

Materials. All chemicals were used as received without further purification. Tetramethylammonium (TMA) and tetraethylammonium (TEA) bromide were obtained from Alfa (98%). Tetrapropylammonium (TPA) bromide was obtained from Fluka (98%) and tetrabutylammonium (TBA) bromide from Aldrich (99%). Potassium permanganate and maleic acid were obtained from Pfaltz and Bauer, 2-butanol (99%) from Aldrich, absolute ethanol from Aaper, and sucrose from United States Biochemical.

Synthesis. Tetramethylammonium (TMA), tetraethylammonium (TEA), tetrapropylammonium (TPA), and tetrabutylammonium (TBA) permanganate salts were made from tetraalkylammonium bromide (TAABr) salts and potassium permanganate according to the literature preparation for $TBAMnO_4$.[39] In a typical synthesis 5.013 g (15.5 mmol) of TBABr dissolved in 20 mL of distilled deionized water (DDW) was added dropwise with stirring to a solution of 2.190 g (13.9 mmol) of $KMnO_4$ in 50 mL of DDW. The resulting purple precipitate was filtered and dried at room temperature to yield 4.7 g of $TBAMnO_4$ (yield 94%). The presence of TAA cations in the permanganate salts was confirmed by IR analysis. The TEA and TPA salts were titrated for total permanganate by reduction to Mn^{2+}, followed by titration to Mn^{3+} with a standard potassium permanganate solution in the presence of pyrophosphate, and found to be stoichiometric.[40] The $TMAMnO_4$ salt was recrystallized from water to prepare a potassium-free salt. The salts were stored in amber bottles away from the light. TMA, TEA, and TPA permanganate salts seem to be stable over a period of months, but the TBA salt readily decomposes to form a gummy dark solid within a few weeks.

Safety Note: The $TAAMnO_4$ salts (TAA = TMA, TEA, TPA, and TBA) decompose passively upon heating at 80−100 °C; however, ammonium permanganate salts with some degree of unsaturation in the organic chain (e.g., $PhCH_2(CH_3CH_2)_3N^+$, $PhCH_2(CH_3)_3N^+$) undergo explosive decomposition at these temperatures.[41] Extreme caution is recommended if unsaturated alkylammonium permanganates are used.

TMA, TEA, and TPA manganese oxide aqueous sols of 0.05−0.2 M manganese concentration were produced by adding the tetraalkylammonium (TAA) permanganate salt to a stirred mixture of DDW and 2-butanol in a ratio varied from 1 DDW to 0.5−2.0 2-butanol with typical volumes of 20−200 mL of each species. In a representative synthesis, a ∼0.05 M Mn aqueous colloid was prepared from the introduction of 0.502 g (2 mmol) of solid $TEAMnO_4$ to a stirred mixture of 40 mL each of DDW and 2-butanol. The mixture was stirred for $^1/_2$ h at room temperature. A dark-red-brown aqueous sol of TEA manganese oxide formed as the lower aqueous layer. The 2-butanol (top) layer was then removed using a separatory funnel. Some residual 2-butanol (up to 20 wt %) is soluble in the water layer.[42] To produce gels, sols were either aged at room temperature for days (0.2 M) to months (0.05 M) or in closed vials at 65−85 °C for several hours to a day. The TBA manganese oxide colloid (0.1 M Mn) is formed in the 2-butanol layer in contrast to the TMA, TEA, and TPA sols. Gels of the TBA manganese oxide colloid were produced by aging at room temperature for several weeks or at 85 °C for several hours in a sealed vial.

Dark-red-brown TMA, TEA, and TPA manganese oxide ethanolic/aqueous sols were prepared in manganese concentrations of 0.05−0.1 M manganese by adding the appropriate $TAAMnO_4$ salt to a mixture of DDW and ethanol in a volume ratio of 40:1 or 2:1 and stirring for $^1/_2$ h. Sols were aged for 4 h to 5 days at room temperature to produce gels, with the longer gelation times required for sols with the higher (40:1) DDW-to-ethanol volume ratio. Samples of 0.1 M sols of TBA were formed for a DDW/ethanol ratio of 2:1, and a precipitate is formed when the ratio of DDW/ethanol is 40:1. Use of neat 2-butanol or ethanol immediately produces a brown gelatinous manganese oxide precipitate for all cations.

TPA manganese oxide aqueous sols and gels were produced using maleic acid or sucrose as reducing agents in water. Sucrose (1 g, 2.9 mmol) was dissolved in DDW (25 mL), and solid $TPAMnO_4$ (0.5 g, 1.64 mmol) was added to form a 0.38 M manganese solution. The mixture was stirred for 2 h to dissolve the permanganate salt, after which time a reddish brown manganese oxide sol formed. The sol gelled within 2 days at room temperature. Maleic acid (0.155 g, 1.3 mmol) was dissolved in 40 mL of DDW, and $TPAMnO_4$ (1.22 g, 4 mmol) was added to produce a 0.1 M manganese solution. A red-brown sol formed after $^1/_2$ h of stirring, and within 2 days it had partially gelled. Addition of another 0.158 g of maleic acid resulted in complete gelation within 5 min.

Average Oxidation State Titrations. The total manganese content of TPA and TEA manganese oxide aqueous sols was determined by removing the soluble alcohol component by gently heating to ca. 70 °C followed by filtration. The resulting sols were dissolved in concentrated hydrochloric and nitric acids, and the Mn^{2+} was titrated to Mn^{3+} in sodium pyrosulfate solution using potassium permanganate.[40] On the basis of the total amount of manganese present, the average oxidation state

of manganese was determined by reduction of the sol to Mn^{2+} with ferrous ammonium sulfate and back-titration of the excess iron with potassium permanganate.[40] Two independent samples were measured for both TEA and TPA colloids. No measurements of average oxidation state were done either for TMA because of the instability of the sol toward gelation or for the TBA sol because the organic component (2-butanol) interferes with the determination.

Elemental Analysis. A Perkin-Elmer model 2380 flame absorption spectrometer or model P40 inductively coupled plasma with atomic emission spectrometer (ICP-AES) was used to confirm the total manganese concentration in the sols and to check for the presence of sodium or potassium in the sols. The sols were dissolved in concentrated hydrochloric and nitric acids and diluted with DDW for the analysis.

X-ray Diffraction Studies. Samples were prepared by pipetting small amounts of the sol onto glass slides and allowing the solvent to evaporate to produce a thin film or by spreading a thin layer of the gel onto a slide. A Scintag XDS-2000 diffractometer utilizing Cu Kα radiation was used to obtain diffraction patterns.

Small Angle Neutron Scattering (SANS) Study. SANS data were obtained on the time-of-flight small-angle diffractometer SAD at the Intense Pulsed Neutron Source (IPNS) of Argonne National Lab.[43] SAD uses pulsed neutrons with wavelengths in the range 0.5−14 Å and a fixed sample-to-detector distance of 1.504 m. The scattered neutrons are measured by using a 64 × 64 array of position-sensitive gas-filled 20 × 20 cm^2 proportional counters, while the wavelengths are measured by time-of-flight by binning the pulse to 67 constant $\Delta t/t = 0.05$ time channels. The instrument thus provides a useful range of momentum transfer ($Q = 4\pi \sin(\theta/\lambda)$, where θ is half the scattering angle and λ is the wavelength of the probing neutrons) of 0.005−0.35 $Å^{-1}$. The reduced data for each sample are corrected for the backgrounds from the instrument, sample cell, and the solvent. The reduced data are placed on an absolute scale by using a polymer melt sample containing an equal-volume mixture of deuterated and hydrogenous high molecular weight polystyrenes whose absolute cross section is known.[43]

Colloidal solutions of TEA manganese oxide were prepared using D_2O/2-butanol, and the residual 2-butanol was removed by rotoevaporation. Samples of 0.40 M concentration of manganese were contained in 2 mm cells. Heating was accomplished ex situ using a water bath at 70 °C for aging of the colloids.

Transmission Electron Microscopy (TEM). Transmission electron microscopy (TEM) data were obtained at 100 kV using a Philips EM420 electron microscope. Samples were prepared by placing a drop of 0.40 M TEA manganese oxide colloidal solution, with the volatile organic component removed by rotoevaporation, on a carbon-coated copper grid and allowing the water to evaporate. The particle size distribution was obtained by measuring the size of ∼80 particles from a film at 300 000 magnification using a magnifying loop with a reticle.

UV/Visible Spectroscopy. UV/visible spectra were obtained on an HP8452A spectrophotometer using a 0.2 cm quartz cell. The sols were diluted to concentrations of between 5×10^{-5} and 5×10^{-4} M Mn for the measurements. Gels were washed and resuspended in water, and the particulate matter was filtered on a coarse frit to produce solutions suitable for spectroscopic studies.

Results

Synthesis and Sol−Gel Transformation. Tetraalkylammonium (methyl, ethyl, propyl, butyl) permanganate precursors were reduced to form manganese oxide colloidal solutions using 2-butanol, ethanol, maleic acid, or sucrose as reducing agents. The reaction of 2-butanol with tetraalkylammonium (TAA) permanganate in water is a two-phase reaction owing to the poor miscibility of the two solvents (2-butanol is soluble in water up to 20 wt %). The TAA permanganate salts have a low solubility in both water and 2-butanol, with the tetramethylammonium salt being the most water-soluble and the tetrabutylammonium salt being the most 2-butanol-soluble. The solid permanganate salts were added to a stirred mixture of 2-butanol and water, and manganese oxide sol formation occurred within $^1/_2$ h. For the tetramethylammonium (TMA), tetraethylammonium (TEA), and tetrapropylammonium (TPA) salts, the reddish-brown manganese oxide colloid forms in the aqueous layer, whereas for tetrabutylammonium (TBA), the colloid is mainly soluble in the 2-butanol layer. The initial sols are pH neutral, but when heated for a few hours or room-temperature-aged for a few weeks the pH increases to >11. The average oxidation state of manganese was determined to range from 3.70 (3) to 3.79 (3) for the TPA and TEA aqueous sols and is consistent with results obtained from XANES studies.[44]

Room-temperature aging of the TEA and TPA manganese oxide sols results in gel formation in anywhere from a few weeks (0.2 M manganese concentration) to several months (0.05 M manganese concentration). The time period required for gelation can be dramatically decreased to 4−24 h by aging of the sols at 65−85 °C in sealed vials. Likewise, TBA manganese oxide 2-butanol sols gel on the time frame of weeks at room temperature and in several hours at 85 °C. However, TMA manganese oxide sols gel rapidly, within a few days to a few weeks at room temperature.

For the TMA, TEA, and TPA sols the aqueous layer retains a certain amount of residual 2-butanol (up to 20 wt %). Complete removal of organic solvent resulted in increased resistance to gelation. Heating for days to weeks, depending on the manganese oxide concentration, was required to effect the sol-to-gel transition. The introduction to the pure aqueous sol of an aliquot of methyl ethyl ketone, acetone, or ethanol equal to 5−10% of the sol volume resulted in gelation within 4 h at 85 °C.

Reduction of the TAA permanganate salts using water/ethanol mixtures likewise produced reddish-brown sols for all TAA cations. In contrast to the above, these sols gel fairly readily at room temperature (within a few hours to a few days). Decreasing the ratio of water to ethanol decreases the time required for gelation, and use of neat alcohols (2-butanol or ethanol) results in immediate formation of a particulate gel or precipitate. With the TPA permanganate salt, aqueous sols are formed with both maleic acid and sucrose and they form dark reddish brown gels within a few days.

Structural Characterization. The formation of long-range order in sols and gels was investigated by X-ray diffraction (XRD). The XRD pattern of a 0.05 M TEA manganese oxide sol prepared by evaporation of the solvent on a glass slide is illustrated in Figure 1. The film, as prepared, consists of manganese oxide in an oily, noncrystalline matrix of TAAOH. Four to six reflections, evenly spaced in 2θ, are observed, in addition to two weak asymmetric reflections at 2.504 and 1.444 Å. The reflections were indexed and refined on a trigonal cell ($P\bar{3}$), as indicated for the TEA case in Table 1, and the pattern is consistent with an expanded birnessite (layered) structure.[45−47] The highest d spacing reflection, the (001), corresponds to the interlayer spacing. Similar patterns are observed for all of the TAA cations studied. Aqueous sols and gels produced using

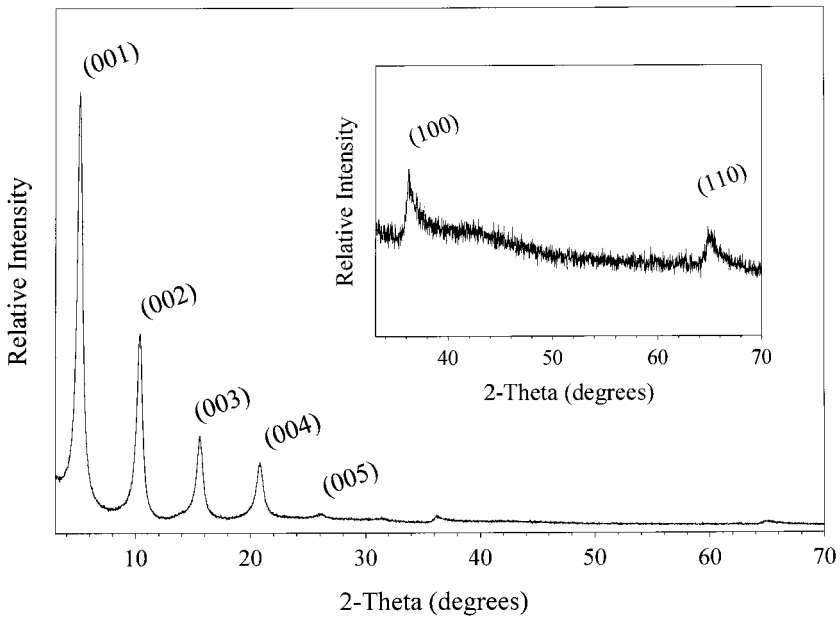

Figure 1. X-ray diffraction pattern of a thin film of TEA manganese oxide on glass prepared by evaporation of solvent from the colloid. The pattern is consistent with a layered manganese oxide structure with tetraalkylammonium cations between the layers, and the reflections have been indexed on a trigonal cell: $a = 2.889$ (1), $c = 17.049$ (13) Å, $\gamma = 120$ °. The (001) reflection corresponds to the interlayer spacing.

TABLE 1: Lattice Parameters and the Observed and Calculated *d* spacings from a Least-Squares Refinement for a TEA Manganese Oxide Structure Produced from Evaporation of TEA Manganese Oxide Colloids onto Glass Slides

space group, trigonal, $P\bar{3}$ lattice constants: $a = 2.889$ (1) Å, $c = 17.049$ (13) Å, $\gamma = 120°$		
hkl indices	obsd *d* spacing (Å)	calcd *d* spacing (Å)
0 0 1	17.059	17.048
0 0 2	8.536	8.524
0 0 3	5.697	5.682
0 0 4	4.264	4.262
0 0 5	3.405	3.409
1 0 0	2.504	2.502
1 1 0	1.444	1.444

2-butanol or ethanol were crystalline, whereas the use of neat alcohols, maleic acid, or sucrose produced amorphous materials.

The observed interlayer spacings are dependent on a number of factors, including the identity of the interlayer cation, the concentration of manganese in the sol, and the aging time and temperature of the sol. The structural transformations in this system are complex; however, a reproducible set of reflections for each cation system can typically be obtained if samples are allowed to age sufficiently and dry completely before the XRD pattern is obtained. Typical XRD patterns are displayed in Figure 2. Generally for TEA, TPA, or TBA, interlayer spacings occur in the range 15−17 Å, whereas for TMA an interlayer spacing of 9.0−9.6 Å is obtained and only two reflections (the second at 4.5−4.8 Å) are observed. Freshly prepared TPA or TBA samples have an initial phase with a (001) reflection at 12.5 and 13.8 Å, respectively, which shifts to 15−17 Å upon heating. XRD patterns obtained from TEA, TPA, and TBA manganese oxide gels typically have an interlayer spacing of 14−15 Å, lower than those of the parent sols. The TMA gels are nearly amorphous.

Freshly prepared manganese oxide sols evaporated onto glass slides initially have broad XRD patterns (Figure 3a). Aging of the sol at room temperature for days to weeks, or at 60−70 °C for a few hours, results in a sharpening of the XRD reflections, as indicated in Figure 3b, consistent with an increase in the

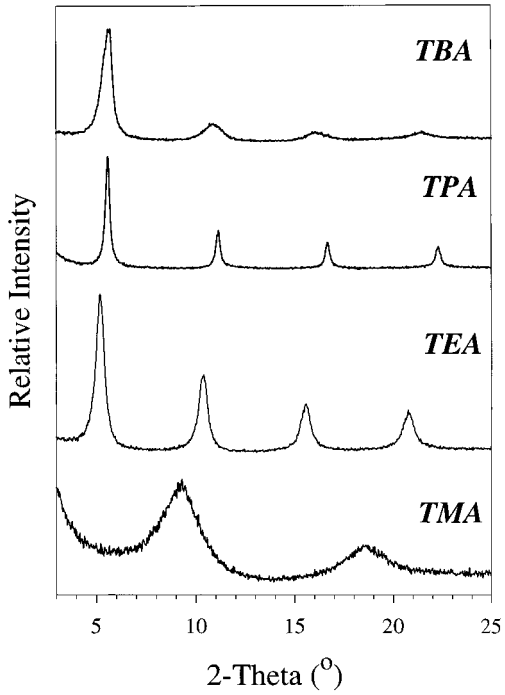

Figure 2. Representative X-ray diffraction patterns obtained from thin films prepared from colloids of the four tetraalkylammonium cations studied. Various interlayer distances have been observed depending on preparation conditions; however, consistent patterns such as these can be obtained if the slides have been briefly heated to 70 °C.

layer stacking order or crystallite size. Gel formation results in a broadening of the XRD reflections as illustrated in Figure 3c, and further aging of the gels for weeks at room temperature or days at 85 °C can result in complete loss of the layer stacking order. The TMA system is unique, demonstrating broad reflections that do not appreciably sharpen upon heating.

As indicated in curves a and b of Figure 4, successive XRD patterns obtained on freshly prepared samples of a TEA manganese oxide gel reveal no XRD reflections when the sample is wet. Upon drying to a paste, broad reflections appear,

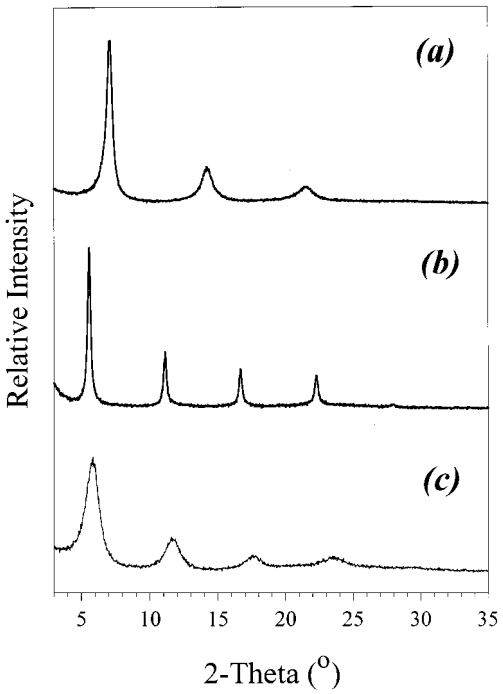

Figure 3. X-ray diffraction patterns obtained from thin films prepared from TPA manganese oxide colloids and gels: (a) freshly prepared colloid; (b) colloid heated at 70 °C for 1 h; (c) gel produced from heating at 70 °C for 12 h.

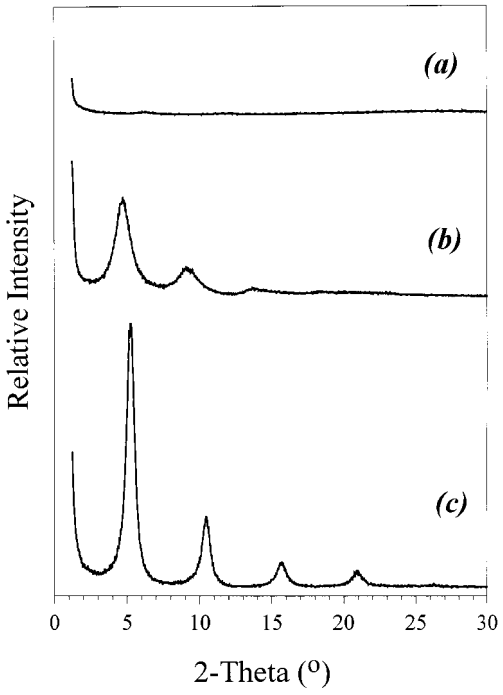

Figure 4. Successive X-ray diffraction patterns obtained from a TEA manganese oxide gel cast onto a slide: (a) wet gel; (b) sample allowed to dry at room temperature; (c) sample annealed at 70 °C for 5 min.

representative of the TEA-incorporated layered structure. Thermal treatment of the evaporated colloid or gel on the glass slide at 60−80 °C for 1 h results in a shift of the interlayer spacing to a characteristic value for each cation, as indicated in Figure 4c for TEA. This is accompanied by a sharpening of the XRD reflections consistent with an increase in long-range order or crystallite size, just as is observed for aging the colloid in solution. TMA sols and gels lose all layer ordering under these conditions, and no shift is observed.

TABLE 2: Effect of Aging Time at 70 °C on the Radius of Gyration (R_g) for Manganese Oxide Particles in a 0.40 M TEA Manganese Oxide Colloid Calculated from a Guinier Plot[a]

aging time (h) 70 °C	R_g (Å)	sphere radius (Å)	H (Å)	L (Å)	H_m (Å)	L_m (Å)
initial	15.7 (11)	20.3 (14)				
2.5	19.7 (11)		15.5 (20)	27.1 (15)	17.0 (12)	31.4 (3)
7.5	24.8 (12)		18.5 (9)	34.3 (17)	14.5 (10)	38.1 (3)
16	34.1 (10)		22.7 (12)	47.3 (25)	16.6 (10)	48.5 (4)
96	53.9 (23)		22.2 (6)	75.7 (32)	12.3 (7)[b]	75.6 (4)[b]
96					13.4 (8)[c]	60.2 (6)[c]

[a] The particle thickness (H) and lamellar radius (L) calculated from a modified Guinier analysis for sheetlike particles and analyzed for a squat cylinder are presented and compared to H_m and L_m for a full profile fit to a squat cylinder. The initial sample is best modeled as a sphere with a radius calculated from the R_g value. [b] Fit at low Q (0.013−0.040 Å^{-1}). [c] Fit at high Q (0.034−0.24 Å^{-1}).

Small Angle Neutron Scattering (SANS). Small angle neutron scattering (SANS) was employed in order to gain information about the kinetics of particle growth and the shape and size of the colloidal particles in solution. A 0.40 M TEA manganese oxide sol free of 2-butanol was produced by concentration (rotoevaporation) of a 0.1 M sol prepared with D_2O. Samples were placed in 2 mm quartz cells, and heating (70 °C) was performed ex situ with a water bath. The scattering data for the initial sample and samples heated for 2.5, 7.5, 16, and 96 h are presented in Figure 5 as log−log plots of the scattering intensity as a function of momentum transfer, Q. The scattering is characterized by a linear region at high Q, which bends over to produce a region of nearly zero slope at low Q. With increased heating time, the scattering intensity increases and the bendover moves to lower Q.

The radius of gyration, R_g, is the root-mean-squared distance of all the atoms from the center of the particle and can be obtained from the data at low Q ($QR_g < 1$).[48] In this region, the scattering intensity $I(Q) = I_o\, e^{-Q^2R_g^2/3}$ and a plot of ln(I) vs Q^2 (Guinier plot) yields a slope proportional to R_g and the y-intercept $I_o = N_P V_P^2(\rho_P - \rho_S)^2$ where N_P is the number of particles in the unit volume, V_P is the volume of the particle, and ρ_P and ρ_S are the scattering length densities of particle and solvent, respectively. These plots, presented as an insert in Figure 5, yield a linear region for all samples studied, and the R_g values are presented in Table 2. For sheetlike particles the scattering data can be analyzed using a modified Guinier approximation for randomly oriented sheetlike particles in solution in which $I(Q) \propto Q^{-2}\, e^{-Q^2R_t^2}$ (R_t is the thickness factor). Plots of ln($I(Q)\, Q^2$) vs Q^2, presented in Figure 6 for samples heated from 2.5 to 96 h, yield linear regions with slopes of $-R_t^2$ from which the plate thickness $H = R_t(12)^{1/2}$ can be calculated. These plots show a shift in the bendover to lower Q values with increased heating time. Values for the plate thickness are presented in Table 2, and the average obtained thickness is ∼20 Å. From the plate thickness, the lamellar dimensions can be estimated using a cylinder model $R_g^2 = L^2/2 + H^2/12$ where L is the radius of the disk. Results range from 27 to 76 Å, depending on the heating conditions, and are presented in Table 2. The initial sample was treated as a spherical particle, $R_{sphere} = R_g(5/3)^{1/2}$, yielding a spherical radius of 20.3 (14) Å.

A fit of the whole scattering profile yields similar results.[49] The fits to the data are presented as lines in Figure 5, and the parameters are given in Table 2. Good fits are obtained for samples heated at 2.5, 7.5, and 16 h. For the sample at 96 h, reasonable fits are not obtained for a full profile refinement.

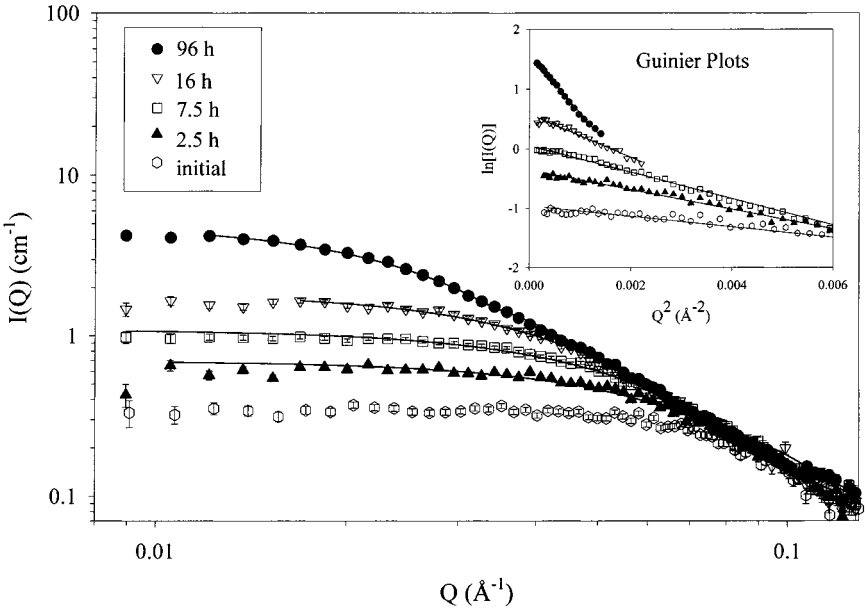

Figure 5. Successive small angle neutron scattering (SANS) data of scattering intensity as a function of momentum transfer (Q) from a 0.40 M TEA manganese oxide colloid. The sample was heated ex situ in a water bath for up to 96 h total heating time. The lines represent fits to a squat cylinder of height H_m and radius L_m and account for incoherant scattering in the background (0.027 cm^{-1}). Guinier plots for all samples are presented in the inset, and the lines represent the linear fits. The results of the fits are presented in Table 3.

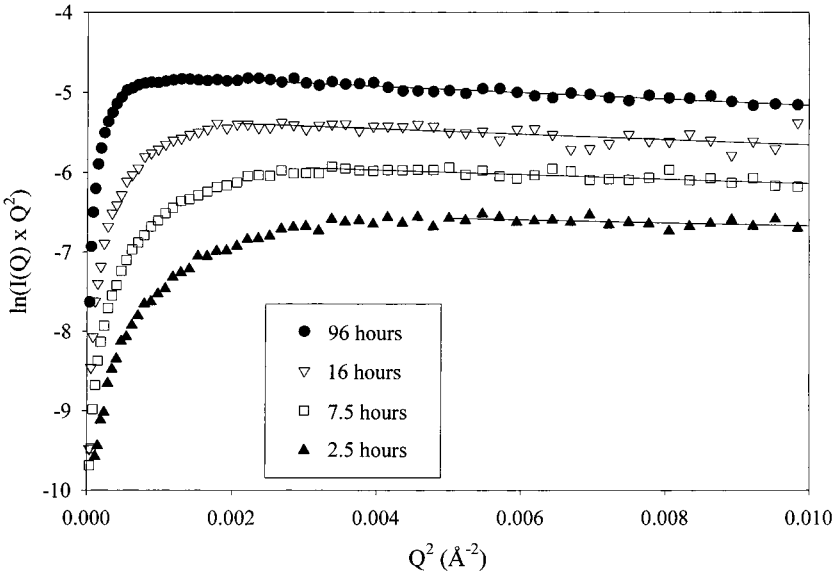

Figure 6. Results of a modified Guinier plot for sheetlike particles for a 0.40 M TEA manganese oxide colloid heated from 2.5 to 96 h at 70 °C. A background subtraction of 0.027 cm^{-1} was applied to the data to account for incoherant scattering. Results of the fit are presented in Table 3.

Instead data were fitted separately in a low-Q region (0.013−0.040 $Å^{-1}$) and a high-Q region (0.034−0.24 $Å^{-1}$). The average thickness H_m is ∼15 Å, slightly smaller than that obtained in the modified Guinier fit. The plate radii, R_m, obtained from the full profile refinement, are in good agreement with those obtained from the radii of gyration.

A plot of R_g as a function of heating time is presented in Figure 7, showing a clear increase in R_g at longer heating times. R_g values range from 15.7 (11) Å for a freshly prepared sample to 53.9 (23) Å for one heated for 4 days at 70 °C. A plot of the plate radius, L or L_m, as a function of heating time yields a similar trend (Figure 7).

One advantage of neutrons over X-rays is the ability to contrast null specific scatterers in the solution, using the ratio of hydrogen (negative scattering length) to deuterium (positive scattering length) in the solvent system. The magnitude of the coherent scattering signal is proportional to the square of the difference of scattering length densities of the particle and the solvent.[50] When the solvent system scattering length density is matched to that of the particles in question, the scattering from these particles can be nulled. The calculated scattering length density for MnO_2 (pyrolusite), based on a density of 5.026 g/cm^3, is $r_P = 2.74 \times 10^{10}$ cm^{-2}, which is equivalent to a 50:50 mixture of D_2O and H_2O. Data were collected on 0.20 M manganese oxide colloids with this solvent system, but no scattering was observed, suggesting the particles formed are a dense MnO_2 phase.

Transmission Electron Microscopy (TEM). TEM data were obtained in order to verify the SANS data with respect to particle size and to gain an idea of the polydispersity of particle size in the samples. Data were obtained on the initial (unheated) sample from the SANS analysis for comparison. A TEM image and particle size distribution histogram for a 0.40 M TEA manganese oxide colloid in which the 2-butanol was removed by roto-

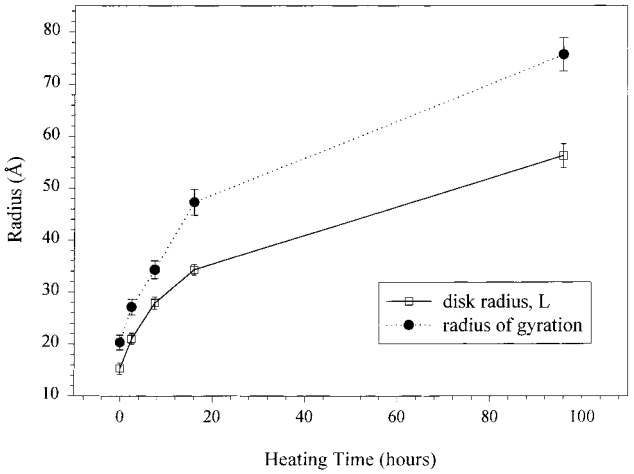

Figure 7. Change in the radius of gyration, R_g, and the spherical (initial sample) or lamellar radius of the manganese oxide particles as a function of heating time for a 0.40 M TEA manganese oxide colloid in which the 2-butanol has been removed by rotoevaporation. L is the radii calculated from the modified Guinier plots and a squat cylinder model, and L_m is the radii obtained from full profile fits to a squat cylinder model.

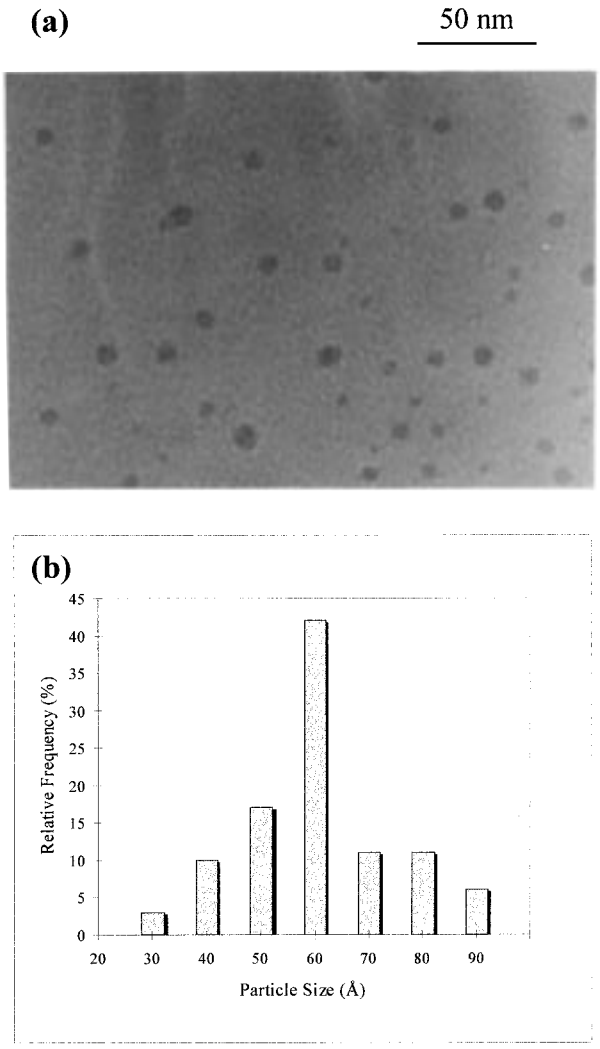

Figure 8. (a) Transmission electron microscope image of manganese oxide nanoparticles prepared from a 0.40 M TEA manganese oxide colloid in which all residual volatile organics have been removed by rotoevaporation. (b) Histogram of particle size illustrating the range of dispersity. The mean particle size is 55.5 ± 1.5 Å.

evaporation are presented in Figure 8. The distribution of particle sizes is a bell curve, with a mean of 55.5 ± 1.5 Å (σ = 13 Å).

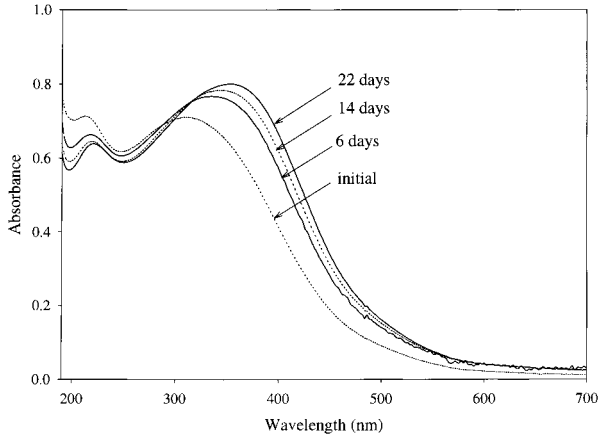

Figure 9. Successive UV/visible spectra of a 0.053 M TEA manganese oxide colloid aged up to 22 d at room temperature. Samples were diluted to a manganese concentration of 5.3×10^{-4} M for the studies.

TABLE 3: Effect of Aging Conditions on the UV/Visible Spectrum of a 0.053 M TEA Manganese Oxide Sol[a]

conditions	λ_1 (nm)	ϵ_1 (mol Mn) × L^{-1} cm^{-1}	λ_2 (nm)	ϵ_2 (mol Mn) × L^{-1} cm^{-1}
freshly prepared	212	6726	312	6700
6 days, 25 °C	218	6254	334	7245
14 days, 25 °C	220	6085	346	7386
22 days, 25 °C	220	6021	354	7545
1 h, 70 °C	218	7085	332	8049
4 h, 70 °C	220	6941	356	8838
7 h, 70 °C	222	6700	368	9960
alcohol-free sol, 1 week, 85 °C	226		377	22020
redissolved gel	222		388	

[a] Samples were diluted to 5.3×10^{-4} M for the studies.

Spectroscopic Studies. The colloids were diluted to concentrations of $(1-5) \times 10^{-4}$ M and examined by UV/visible spectroscopy. The position and intensity of the absorbance bands are monitored as a function of aging time at room temperature (Figure 9) and 70 °C for a 0.053 M aqueous TEA sol. The absorbance maxima and absorptivities are presented in Table 3. Freshly prepared colloids have a broad absorbance band with a maximum (λ_1) at 312 nm and an absorbance tail out to 600 nm. Additionally, there is a weaker absorbance band (λ_2) at 212 nm. Both bands shift to lower energy upon aging at room temperature for days to weeks, or at 70 °C for hours. In addition to the energy shift in the absorbance bands, there is also an increase in absorptivity for the lower energy band (λ_1) and a decrease for the higher energy band (λ_2) as the samples are aged. The greatest shifts are generally observed for the gel that has been redissolved by agitation for several hours in water. A plot of absorbance as a function of concentration in the region 5×10^{-5} to 5×10^{-4} M TEA manganese oxide for the freshly prepared sol obeyed Beer's law, and no shift of λ_1 or λ_2 was observed in this concentration range. The samples diluted to concentrations of $(1-5) \times 10^{-4}$ M Mn for the UV/vis studies showed only small changes in absorbance maxima (2−5 nm) or absorptivity (70−500 (mol Mn) L^{-1} cm^{-1}) over a period of weeks at room temperature.

The TPA manganese oxide sols show the same trend as a function of aging conditions as the TEA sols. The UV/visible data for a 0.046 M Mn sol as a function of aging time at room temperature are presented in Table 4. The absorbance maxima are at lower energies than those observed for the TEA manganese oxide sols, and they do not shift as quickly or to the same extent.

TABLE 4: Effect of Room-Temperature Aging on the UV/Visible Spectrum of a 0.046 M TPA Manganese Oxide Sol[a]

conditions	λ_1 (nm)	ϵ_1 (mol Mn) × L^{-1} cm^{-1}	λ_2 (nm)	ϵ_2 (mol Mn) × L^{-1} cm^{-1}
freshly prepared	206	7633	294	7207
6 days, 25 °C	208	7236	296	7116
14 days, 25 °C	216	6365	328	7417
22 days, 25 °C	216	6329	334	7384

[a] Samples were diluted to 4.6×10^{-4} M for the study.

Discussion

Synthesis of Manganese Oxide Colloids. There are a variety of successful techniques for the synthesis of nanocrystals and nanostructured materials, including reverse micelle syntheses and template or guest−host syntheses using membranes or zeolites.[51] Difficulties in the preparation of nanoparticles of manganese oxide lie in their strong tendency to condense, a tendency due in large part to the presence of hard metal cations in the synthesis that promote the condensation. The ability to make colloidal "jellies" of manganese oxide through reduction of permanganate salts using sugars and various other organic compounds has been noted for a long time,[52] and recently, these gels have been reinvestigated, resulting in new synthetic routes to both layered and tunnel manganese oxide materials.[36,53−57] Coagulation or condensation remains a problem in these systems. A better way to control the nucleation process and prevent association is needed in order to prepare nanocrystals. A promising route to nanocrystals of manganese oxide may be found by replacement of hard cations in the synthesis procedure with soft organic cations, such as tetraalkylammonium cations, which have been shown to successfully control condensation in a variety of other nanocrystal syntheses.[58] Incorporation of the tetraalkylammonium moiety into the starting permanganate salt followed by reduction with organic alcohols is a successful and facile strategy for the preparation of crystalline nanoparticles of manganese oxide with well-defined sizes.

$TAAMnO_4$ (TAA = TMA, TEA, TPA, TBA) salts were prepared and isolated from the reaction of TAABr and $KMnO_4$ salts in water and subsequently reacted with a variety of organic reagents to prepare reddish-brown manganese oxide colloidal solutions. Manganese oxide sols were formed with maleic acid, sucrose, ethanol, and 2-butanol as reducing agents. The initial ratios of $TAAMnO_4$ to sucrose or maleic acid were chosen to mimic sol−gel reactions with $KMnO_4$, which ultimately produced a layered manganese oxide (birnessite) for sucrose and a tunnel-structured material (cryptomelane) for maleic acid.[53−56] The maleic acid is added stoichiometrically on the basis of the mechanism and a desired oxidation state between 3.5 and 4 of manganese,[36] whereas the sucrose is added in large excess. The reaction of secondary alcohols to ketones with permanganate salts to produce Mn^{4+} or Mn^{3+} oxides is described below in eq 1 (Mn^{4+}) and eq 2 (Mn^{3+}):

$$2MnO_4^- + 3RCH(OH)R' \rightarrow 2MnO_2 + 3R(C{=}O)R' + 2H_2O + 2OH^- \quad (1)$$

$$MnO_4^- + 2RCH(OH)R' \rightarrow MnO_2^- + 2R(C{=}O)R' + 2H_2O \quad (2)$$

Primary alcohols can be expected to react in a similar manner, producing aldehydes and carboxylic acids.

The presence of mixed-valent manganese (between +3 and +4) results in residual negative charge on the manganese oxide lattice, assuming a minimum of oxygen deficiencies. Anywhere from a few equivalents to a large excess (on the order of 10^3) of 2-butanol or ethanol can be used in the reactions, but higher concentrations of alcohol result in faster reaction times (on the order of minutes). Nevertheless, the average oxidation states of aqueous sols of TPA and TEA manganese oxides were in the range 3.70−3.79, suggesting that the oxidation state of manganese is determined by the reducing ability of the organic reagent. Continued heating with the organic reagent above 100 °C will result in reduction of the manganese oxide as indicated by a change in color to light brown and the identification of γ-Mn(O)OH (manganite) by X-ray diffraction. The control of oxidation state by the reducing ability of the organic reagent is also observed in the reaction of sucrose with $KMnO_4$; even with the large excess of sucrose present, the average oxidation state of manganese remains above 3.5.[53] Active forms of manganese oxide are frequently used as oxidizing agents in organic syntheses; however, the activity is strongly dependent on synthetic conditions.[59] Under the conditions in which the TAA-containing colloids are prepared, manganese oxides with oxidation states near 4 are stable in the presence of organic species with alcohol, aldehyde, and alkene functional groups at room temperature.

Successful formation of a stable manganese oxide sol in the TAA system is due to the absence of metal cations, which have long been known to have a coagulating effect on manganese oxide sols,[37] as well as the dispersive ability of the TAA cations, which act to keep manganese oxide colloidal particles apart. Consistent with this analysis, addition of small amounts of sodium or magnesium salts to TAA manganese oxide sols induces immediate precipitation of manganese oxide phases.

Sol−Gel Transformation. Gelation, which occurs rapidly in the $KMnO_4$ maleic acid or sucrose systems, can be well controlled by use of TAA cations in the synthesis matrix. In the TAA system, the gel time is dependent on a number of factors including the size of the TAA cation, the amount of organic reducing phase present in the sol, manganese concentration, and the temperature.

The effect of the TAA cation on the sol−gel properties depends on the size of the monovalent cations. For aqueous solutions of the same concentration under the same conditions, the order of gelation as a function of TAA cation is as follows: TMA ≫ TEA > TPA. Association between the negatively charged manganese oxide particles is governed by the ability of the cation to counter this negative charge through association. Thus, the smaller cations have less dispersive ability and manganese oxide colloids prepared with TMA gel the quickest. For the sucrose and maleic acid system, it is also possible to compare the gelation time for an alkali metal cation relative to a tetraalkylammonium cation. Consistent with the proposed dependence on size, it takes several days for a gel to form in the TPA system relative to a few minutes to an hour in the potassium system.[37,54−56]

The presence of residual or added organic reducing agents increases the propensity toward gelation. Removal of the residual 2-butanol component from aqueous sols of TEA or TPA by rotoevaporation or heating produces sols that are more stable toward gelation and in some cases do not gel after heating for months. These colloids can be induced to gel by subsequent addition of ethanol, 2-butanol, or 2-butanone. The fact that gels form with simple alcohols is in contrast to the potassium permanganate system above, in which sols and gels are only

formed for maleic acid, sugars, and polyols. Simple alcohols such as ethanol and 2-butanol induce precipitation of manganese oxide when reacted with potassium permanganate.[54] Multifunctional organic agents may be necessary for the formation of a cross-linked gel network and to prevent precipitation of manganese oxides in the presence of alkali metal cations.[54] However, in the TAA system, even with simple alcohols the sols will form gels, indicating that multifunctional organic components are not necessary for manganese oxide condensation.

In the 2-butanol system, room-temperature aging of aqueous manganese oxide sols with TEA and TPA forms gels, but the process is very slow. For low manganese concentrations (0.05 M or lower), gelation can take several months, whereas for concentrations of 0.2 M, gelation takes place within several weeks. The most rapid formation of a gel occurs upon heating the sols in closed vials at 65−85 °C, decreasing the gel time to a duration of a few hours to 1 day. This suggests that condensation or agglomeration is accelerated with increasing temperature and manganese concentration. The aging process is accompanied by an increase in pH. Initial sols are pH neutral but become basic over a period of days at room temperature or hours at 65−85 °C. This formation of hydroxide is consistent with the known mechanism for the reaction of permanganate salts with alcohols (see eqs 1 and 2).

Manganese Oxide Structures in Solutions and in Thin Films. The presence of a crystalline phase within the colloids prepared by reduction with alcohols is the first indication that a crystalline phase can be obtained in the manganese oxide system by a sol−gel method without subsequent heating. Other sol−gel experiments with manganese oxides using $KMnO_4$ and sucrose or fumaric/maleic acids produce an amorphous phase at room temperature. Heating of the gel above 350 °C is required for the formation of crystalline phases.[36,53−56] Our studies with $TAAMnO_4$ salts reported here, as well as those of Bach et al.,[36] indicate that the reaction of these salts with sucrose and maleic or fumaric acid likewise produces amorphous phases at room temperature.

The process of self-assembly occurs upon evaporation of the colloid onto flat surfaces or gelation, resulting in layered structures in which slabs of manganese oxide are separated by cations and water. The lamella are composed of CdI_2-type edge-sharing MnO_6 octahedra, and the structures produced can be modeled as an expanded hexagonal birnessite.[45,60] The structure has been confirmed by EXAFS studies[44] and is similar to a number of other layered materials found in the transition metal sulfide,[61] oxide,[32,33,62−65] and phosphate systems.[66] The high intensities of the (00*l*) reflections relative to the (100) and (110) are a direct result of the preparation technique resulting in strong preferred orientation due to the lamellar particles settling on their *c* faces. The thin film samples reported here are not appropriate for detailed compound investigation, because of the matrix of TAAOH, 2-butanol, and water. Studies are underway on washed and dried gels and will be the subject of another paper.

Proposed structural models consistent with the observed interlayer spacings are presented in Figure 10, and the assignment of observed TAA manganese oxide phases is indicated in Table 5. Calculated interlayer spacings are based on the dimensions of the manganese oxide layer, the van der Waals radius of water, and the size of the TAA cations. Model I assumes the absence of a hydration layer between the TAA cation and manganese oxide layers, although water molecules may be present in the same plane as the TAA cations. Model III represents an expansion of 5.6 Å relative to model I, consistent with water layers between the TAA cation and the

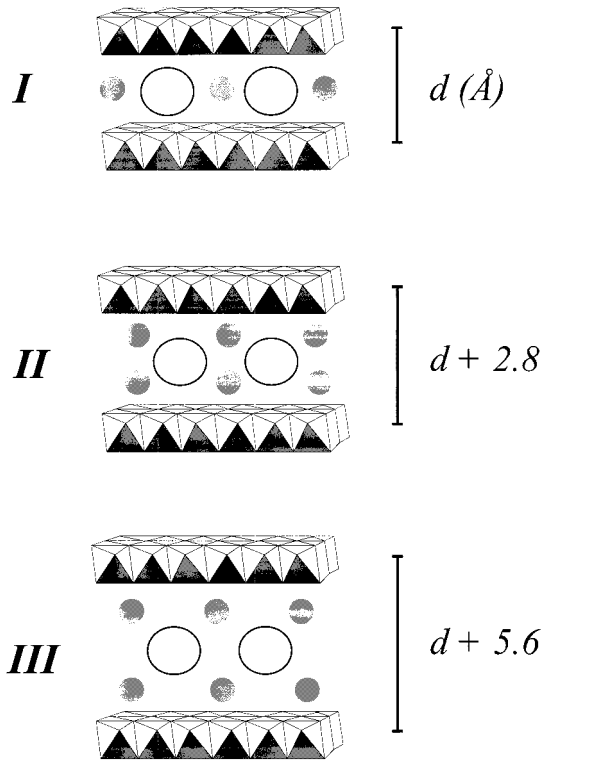

Figure 10. Illustration of simple structural models for the TAA-occluded manganese oxide colloids based on zero, one, and two layers of hydration between the cation and manganese oxide layers. The large spheres represent TAA cations and the small gray spheres water.

TABLE 5: Correspondence of the Predicted Interlayer Spacing from the Structural Models Presented in Figure 5 with the Observed Interlayer Spacing for TBA, TPA, TEA, and TMA Incorporated Manganese Oxide Colloids[a]

cation	cation size[b] (Å)	inclusion model	predicted interlayer spacing (Å)	obsd interlayer spacing (Å)
TBA	9.5−10.5	I	14−15	13.8
		II	16.8−17.8	16.6
TPA	8−9	I	12.5−13.5	12.5
		II	15.3−16.3	16.0
TEA	6.5−7.5	III	16.6−17.6	17.0
TMA	6.0	collapsed structure		9.0−9.6

[a] Based on manganese oxide slab thickness of 4.5 Å and a van der Waals radius of water of 2.8 Å. [b] Szostak, R. *Molecular Sieves: Principles of Synthesis and Identification*; Van Nostrand Reinhold: New York, 1989; p 95.

manganese oxide slabs. The intermediate model, model II, corresponds to a total of one effective layer of water (2.6 Å) in addition to the TAA cations. Interlayer spacings consistent with model II are only observed for the larger cations TPA and TBA and may be due to the arrangement of the water molecules in the hydration sphere of these cations, or partial interleaving of water molecules between the alkyl chains.

Organic cation incorporation into layered structures has been observed in a number of systems.[32,64,66−69] Among the manganese oxides, phyllomanganates similar to those that self-assemble as thin films in the TAA manganese oxide colloidal system described here have been reported from exchange of long-chain alkylammonium cations into birnessites. Interlayer spacings of up to 25.6 Å are obtained for the intercalation of dodecylammonium.[70] Exchange of dodecylammonium has made possible the incorporation of Keggin ions to form pillared birnessites.[46] In situ preparations of birnessites via oxidation of $Mn(OH)_2$ in the presence of dodecyltrimethylammonium hy-

droxide have likewise produced intercalates with interlayer spacings of 25.4 Å.[71] However, these previously reported expanded phyllomanganates are fundamentally different from the ones reported here, owing to their large crystallite size.

SANS studies have indicated that the manganese oxide lamella are not formed during the evaporation process but are formed in solution. However, the manganese oxide/tetraalkylammonium cation sandwich-type layer structures do appear to be a consequence of the evaporation process. A linear region is observed in the modified Guinier plot (Figure 6) for samples heated 2.5 h or more, suggestive of particles with a platelike shape, and the full pattern can be modeled as a squat cylinder with thicknesses of 15−20 Å. This thickness is consistent with the *c* parameter observed in the thin film TEA manganese oxide intercalates (17.0 Å). Thus, it appears that the lamella are aggregated to a small extent, resulting in MnO_x/TEA/MnO_x sandwiches in solution. This is in contrast to the null scattering experiment that suggests that the manganese oxide sol has the same scattering length density as pyrolusite (β-MnO_2), consistent with the scatterers having a structure of a condensed-phase manganese oxide rather than the low-density structure of TAA intercalated manganese oxides. Since the null scattering experiments were performed at a lower manganese oxide concentration than the aging studies, it is possible that the assembly of lamella into sandwich structures only occurs above a critical concentration.

The formation of intercalated structures only at high concentrations or upon evaporation is consistent with XRD results. XRD patterns of wet samples, such as the one presented in Figure 4a, show no diffraction, suggesting that the layers are self-assembling with the tetraalkylammonium cations directly on the glass slide and do not achieve structural order until nearly all the solvent has been removed. The fact that little or no association is observed in solution can be attributed to the weak interactions between the negatively charged manganese oxide particles and the large tetraalkylammonium cations and is the same effect responsible for the stability of the colloidal system to coagulation or precipitation. The ability to associate and delaminate layered structures has been observed in a number of clay systems, disulfides, and more recently, in some perovskite type niobates and titanates.[66,68,72−74] Significant attention has been focused on delamination of layered structures because in their delaminated form they readily undergo ion exchange and can be used for the formation of nanocomposite materials.[75]

The interlayer spacings resulting from the evaporation of colloids onto glass slides, or in the gels, are very sensitive to the treatment history of the colloid and the evaporation process. The manganese oxides produced with larger cations (TBA, TPA) show a greater diversity of interlayer spacings than the smaller cations (TEA, TMA). The TBA and TPA systems have an initial structure associated with freshly prepared manganese oxide colloids. The interlayer spacings observed in these structures are 13.8 and 12.5 Å, consistent with tetraalkylammonium cations sandwiched between layer structures with no associated layers of water shielding the TAA cations from the manganese oxide layers (model I, Figure 10). Such structures have been observed for layered TiO_2 with TBA as intercalant.[73] The relatively poor stability of this structure is demonstrated when the colloid is heated or aged at room temperature or the slide with the deposited film is heated, resulting in a swelling of the layers to 16.6 and 16.0 Å for TBA and TPA, respectively. The difference in the interlayer spacings between these two phases amounts to 2.5−2.8 Å and corresponds to the van der Waals radius of a single water molecule (2.8 Å).[62] This may result from a structural rearrangement of water molecules around the cations to produce a buffer between the cations and the manganese oxide slabs or from the uptake of additional water from the environment. The net effect in terms of interlayer spacing is a half-layer of water on either side of the cation (model II, Figure 10). This effect may be attributed to the structure of the hydration sphere for TPA or TBA or the partial interleaving of water molecules between the alkyl chains.

In contrast to the TPA and TBA cases, thin films prepared from evaporation of the TEA manganese oxide colloid generally produce only a single phase. Despite the small size of TEA (6.5−7.5 Å) relative to TPA (8−9 Å) and TBA (9.5−10.5 Å), the interlayer spacing for the TEA manganese oxide structure is larger than that for the TPA and TBA manganese oxides. For TEA manganese oxide, an interlayer spacing of 17.0 Å is obtained and corresponds to two hydration layers of water, in addition to the TEA cation, between the layers (model III, Figure 10). This structure is analogous to the structure of Mg−birnessite, a phyllomanganate in which the cation is surrounded by a sphere of hydration.[76]

The TMA cation is unique in this series in that the structures formed in thin films of TMA manganese oxide are poorly ordered as indicated by the broad peaks obtained in the XRD pattern. While indicative of a layered structure, the interlamellar spacing of 9−9.6 Å is too small to reflect a simple TMA intercalate based on model I (10.5 Å), II (13.3 Å), or III (16.1 Å). Decomposition of TAA cations under strongly basic conditions has been noted;[77] however, infrared studies and C, H, N analysis suggest that the TMA cation remains intact in the manganese oxide colloid.[78] The pattern is very similar to those obtained when dried gels of TBA, TPA, and TEA are ground, and it is likely that it arises from a collapsed structure in which TMA cations are no longer intercalated between the layers.[79] This is in direct contrast to the well-defined layered structure obtained with TMA in the vanadium oxide system.[69]

The size of the cations and their hydration sphere are different in solution than when trapped between the layers of manganese oxide, as reported here. In solution, TBA is the most hydrophilic and TMA the least, and the size of the hydrated cation scales with the size of the nonhydrated cation.[80−82] However, another factor that may come into play is the effect of the cation on the water structure in the hydrating layer. In aqueous solutions, TBA and TPA are known to be structure makers, promoting the formation of a hydrogen-bonded network of the water molecules in their vicinity.[80−82] TMA is a structure breaker, and TEA is neutral. Thus, TBA and TPA may be expected to have a hydration sphere that is ordered differently from that of TEA or TMA. Furthermore, the longer alkyl chains of the TBA and TPA cations may permit some nesting of the water.[80] The structural ordering, nesting, or a combination of the two effects may explain why the TEA cation results in interlayer spacings increased by 5.6 Å over that predicted from a naked TEA cation, whereas TPA and TBA have an interlayer spacing reflective only of the TAA cation or expanded by 2.8 Å.

Some sense of the disorder in the self-assembled structures can be probed by XRD. The asymmetric line shape observed for the (100) and (110) reflections is indicative of turbostratic stacking,[83] in which the hexagonal lattice of one layer is rotated about *c* relative to the lattice of the adjacent layer and/or translated in the *ab* plane. This is a common short-range order effect observed in a number of clays.[84] The general broadening of the (00*l*) reflections can arise from variation in the interlayer spacing or small crystallite size. Some assessment of the interlayer order can be made by comparing peak broadening in samples under different treatment conditions. Generally, freshly

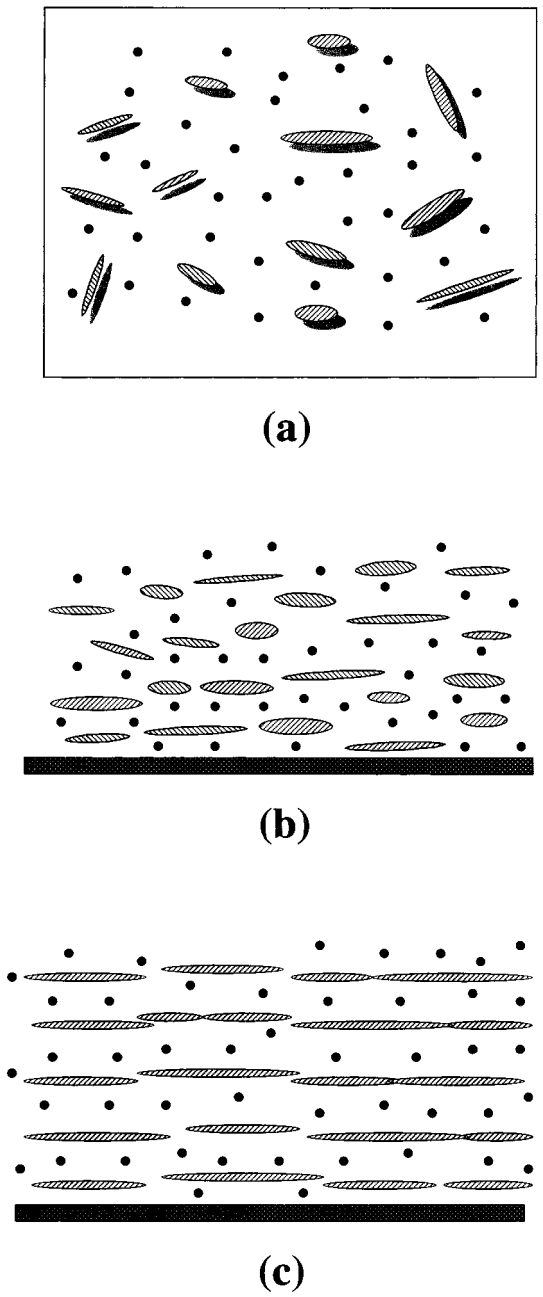

Figure 11. Schematic illustration of the self-assembly process that takes place on glass slides to produce a layered manganese oxide structure with tetraalkylammonium cations intercalated between the layers: (a) unassociated particles free-floating in solution; (b) initial structure, consisting of small regions of crystallinity, formed from evaporation of colloids onto glass slides; (c) well-ordered structure produced from heating the colloid in solution or annealing the thin film sample described in (b). The disks represent the negatively charged disklike manganese oxide particles, and the filled black circles are the tetraalkylammonium cations.

prepared samples have broader reflections than thin film samples that have been annealed, indicating more disorder. A scheme for the self-assembly process on glass slides is presented in Figure 11. Initially, manganese oxide plates are largely free floating in solution. Upon evaporation on a glass slide, layer stacking occurs; however, there is a large degree of disorder, resulting in the broadening of the (00*l*) reflections. Annealing of the samples permits the plates to rearrange, resulting in larger areas of order and the concomitant sharpening of the XRD reflections. Relatively narrow XRD peaks are also obtained when the colloids are heated in solution prior to deposition on glass slides. In this case, the increase in order is probably a function of an increase in the lamellar radius (vide infra), which may facilitate stacking within the structure.

Quantum Confinement Effects and Particle Growth of Nanocrystalline Manganese Oxides. The optical properties observed in semiconducting nanocrystals are a direct result of quantum confinement effects that arise when the size of the particle becomes smaller than the exciton (electron−hole pair) in the bulk material.[85] The exciton is in fact in an excited state, and quantized levels arise from the band diagram of the bulk, with a band gap that is size-dependent. Thus, optical absorbance is a powerful tool to probe particle size and particle growth when the semiconducting crystallites are on the order of nanometers in size.

For the manganese oxide colloidal system, two absorbance bands are observed that shift in energy and intensity as a function of time. These consist of a high-energy band near 220 nm and low-energy band in the region 290−390 nm with a broad tail out into the visible. It is this broad tail that is responsible for the intense red-brown color of the colloid. Both bands shift to the red with time, although the lower energy band has a more pronounced shift, and the absorptivity of the lower energy band increases, whereas that of the higher energy band decreases. Similar bands have been observed in discrete Mn(IV) complexes with alkoxy ligands and attributed to charge-transfer bands.[86] Given the high molar absorptivities (6000−22 000 (mol Mn) L^{-1} cm^{-1}), it is reasonable to assign the bands in the manganese oxide colloidal particles in a similar manner. Such absorbances have also been observed in other manganese oxide colloidal systems, including those produced by γ-irradiation of $KMnO_4$[23] and those prepared by reaction of $KMnO_4$ with organic compounds containing carbon−carbon double bonds,[25] and similar to the data presented here, the bands were observed to shift to lower energy with aging time. However, these studies were performed with colloids of very dilute concentrations (1×10^{-5} M), whereas those presented here can be prepared and are stable in concentrations as high as 0.57 M because of the dispersive effect of the tetraalkylammonium cations.

These absorbances occur at a lower wavelength than that observed for bulk manganese oxide, which has a maxima at 400 nm,[87] and are consistent with quantum confinement due to the small particle size. The shift with respect to time suggests that the particles are growing, resulting in a decrease in the band gap. This is consistent with the greater degree of order observed in heated colloids evaporated onto glass slides, as larger lamella would be expected to form a more ordered structure, and consistent with the tendency of the system to gel rapidly upon heating, which can be attributed to the particles attaining a critical size. As illustrated by the absorbance data in Table 3, such growth is more pronounced at high temperature, suggesting that increased temperature results in an increased rate of condensation or agglomeration. The smallest energy gap, corresponding to the largest particle size, is observed for a gel that has been temporarily resuspended by vigorous shaking. Apparently, once the particle size has become sufficiently large to gel, there can be no reversal through hydrolysis or deflocculation, or such a reversal is temporary. Within a few days flocculant fibrous particles settle out of the dilute solution into which the gel has been resuspended.

The growth is also dependent on the identity of the TAA cation. A comparison of the room-temperature data from Tables 3 and 4 reveals that growth occurs more rapidly in the TEA system than in the TPA system. This is consistent with the smaller size of the TEA cation being less effective at dispersing

the manganese oxide particles or being more effective at balancing charge on the manganese oxide particles, permitting more facile condensation.

The interpretation of the shifts observed in the UV as due to an increase in the size of the absorbing particle (a decrease in the band gap) has been confirmed with the SANS study. To get sufficient scattering, more concentrated solutions (0.40 M TEA manganese oxide) were studied, and the volatile organic component was removed by rotoevaporation, since coherent scattering due to small bubbles of 2-butanol was found to interfere with the analysis. There is a clear increase in the particle size with heating time at 70 °C. The shift in bendover in both the *I* vs *Q* (Figure 5) and modified Guinier plots (Figure 6), as well as the increase in scattering intensity with heating time, is consistent with particle growth. The particle sizes range from 20 to 80 Å in radius, which is within the size range from which one would expect to observe quantum confinement effects.

The change in particle size decreases with increasing heating time (Figure 7), consistent with a mechanism of agglomeration in which small nuclei are assembled together to create larger particles.[88] Furthermore, since the increase in R_g and L occur by the same factor over time, it is clear that the particles are growing only in two (lateral) dimensions. This is confirmed by the absence of a significant change in the layer thickness with heating time. In this system, it would appear that formation of nuclei occurs during a brief induction period. UV/visible spectra taken $^1/_2$ h after dissolution of the tetraalkylammonium permanganate salt into the water/2-butanol mixture indicate that all of the permanganate has been consumed; i.e., nucleation is rapid and ceases in a short period of time. As the small nuclei are depleted over time, the particle size levels off, principally because of the fact that agglomeration and/or condensation between large particles is not favored.[88] However, it is possible to slow or quench the particle growth in the system through dilution of the colloid. When diluted to manganese concentrations of $\leq 1 \times 10^{-4}$ M, only small shifts (2−5 nm) were observed in the absorbance of the colloid over a time period of several weeks, consistent with significantly arrested particle growth.

Consistent with a mechanism of fast nucleation at short heating times, samples of nanocrystalline manganese oxide with relatively low polydispersity can be obtained. TEM micrographs reveal disklike or spherical particles with an average radius of 27.8 (7) Å and a standard deviation of 6.5 Å. The radius obtained by TEM is slightly larger than that obtained for the freshly prepared colloid from SANS data (20.3 (14) Å). Excellent fits of the SANS data are obtained for samples heated to 16 h. Lamellar radius values vary between 27 and 31 Å for a 0.40 M TEA manganese oxide colloid heated for 2.5 h at 70 °C and 47−49 Å when heated for 16 h. At 96 h of heating a large radius range of 60−76 Å is obtained, arising from the need to fit the low- and high-*Q* data separately to obtain a good fit. This is an indication of polydispersity in this sample, suggesting that short heating times are advantageous for the preparation of monodisperse samples.

Conclusions

A simple route has been developed for the preparation of novel mixed-valent manganese oxide nanocrystals with good particle size control. The key to the stabilization of the colloids is the incorporation of tetraalkylammonium cations into the synthesis and the exclusion of hard metal cations such as alkali metals and alkaline earths. These manganese oxide colloids represent a unique semiconducting system in which quantum confinement effects have not been explored. Furthermore, they are prepared in a delaminated form and can undergo self-assembly to produce layered structures. This combination of physical properties and the facility of ordered structure formation make these colloids promising starting materials for the design of sensors, catalysts, and battery materials. Future work will focus on luminescence properties of the colloids, the effect of alcohols on particle growth, characterization of the TAA manganese oxide gels, and the preparation of thin films from the colloidal solutions for catalytic and electrochemical applications.

Acknowledgment. The authors acknowledge the initial SANS studies of Dr. Dianna Young on this system. The assistance of Dr. Lennox Iton, Dr. Kathleen Carrado, Dr. Kenneth Littrell, and Mr. Denis Wozniak at Argonne National Lab and Ms. Wei Tong at the University of Connecticut with the SANS studies presented here is greatly appreciated. The support of the U.S. Department of Energy, Office of Basic Energy Sciences, Division of Chemical Sciences is gratefully acknowledged.

References and Notes

(1) (a) Steigerwald, M. L.; Brus, L. E. *Acc. Chem. Res.* **1990**, *23*, 183−188. (b) Alivisatos, A. P. *J. Phys. Chem.* **1996**, *100*, 13226−13239.

(2) Bley, R. A.; Kauzlarich, S. M. *J. Am. Chem. Soc.* **1996**, *118*, 12461−12462.

(3) Zhang, L.; Coffer, J. L.; Xu, W.; Zerda, T. W. *Chem. Mater.* **1997**, *9*, 2249−2251.

(4) (a) Peng, X.; Wilson, T. E.; Alivisatos, A. P.; Schultz, P. G. *Angew. Chem., Int. Ed. Engl.* **1997**, *36*, 145−147. (b) Counio, G.; Esnouf, S.; Gacoin, T.; Boilot, J.-P. *J. Phys. Chem.* **1996**, *100*, 20021−20026.

(5) (a) Micic, O. I.; Sprague, J. R.; Curtis, C. J.; Jones, K. M.; Machol, J. L.; Nozik, A. J.; Giessen, H.; Fluegel, B.; Mohs, G.; Peyghambarian, N. *J. Phys. Chem.* **1995**, *99*, 7754−7759. (b) MacDougall, J. E.; Eckert, H.; Stucky, G. D.; Herron, N.; Wang, Y.; Moller, K.; Bein, T.; Cox, D. *J. Am. Chem. Soc.* **1989**, *111*, 8006−8007. (c) Li, Y.-D.; Duan, X.-F.; Qian, Y.-T.; Yang, L.; Ji, M.-R.; Li, C.-W. *J. Am. Chem. Soc.* **1997**, *119*, 7869−7870. (d) Janik, J. F.; Wells, R. L.; Young, V. G., Jr.; Rheingold, A. L.; Guzei, I. A. *J. Am. Chem. Soc.* **1998**, *120*, 532−537. (e) Guzelian, A. A.; Katari, J. E. B.; Kadavanich, A. V.; Banin, U.; Hamad, K.; Juban, E.; Alivisatos, A. P.; Wolters, R. H.; Arnold, C. C.; Heath, J. R. *J. Phys. Chem.* **1996**, *100*, 7212−7219.

(6) (a) Nyffenegger, R. M.; Craft, B.; Shaaban, M.; Gorer, S.; Erley, G.; Penner, R. M. *Chem. Mater.* **1998**, *10*, 1120−1129. (b) Sunstrom, J. E., IV.; Moser, W. R.; Marshik-Guerts, B. *Chem. Mater.* **1996**, *8*, 2061−2067. (c) Yin, J. S.; Wang, Z. L. *J. Phys. Chem. B* **1997**, *101*, 8979−8983. (d) Masui, T.; Fujiwara, K.; Machida, K.; Adachi, G.; Sakata, T.; Mori, H. *Chem. Mater.* **1997**, *9*, 2197−2204.

(7) (a) Murray, C. B.; Kagan, C. R.; Bawendi, M. G. *Science* **1995**, *270*, 1335−1338. (b) Hu, K.; Brust, M.; Bard, A. J. *Chem. Mater.* **1998**, *10*, 1160−1165. (c) Moffitt, M.; Vali, H.; Eisenberg, A. *Chem. Mater.* **1998**, *10*, 1021−1028. (d) Connolly, S.; Fullam, S.; Korgel, B.; Fitzmaurice, D. *J. Am. Chem. Soc.* **1998**, *120*, 2969−2970.

(8) Caneschi, A.; Gatteschi, D.; Sessoli, R. *J. Chem. Soc., Dalton Trans.* **1997**, 3963−3970.

(9) Besenhard, J. O. In *Soft Chemistry Routes to New Materials—Chimie Douce*; Rouxel, J., Tournoux, M., Brec, R., Eds.; Trans Tech: Aedermannsdorf, 1994; pp 152−153.

(10) Suib, S. L. In *Studies in Surface Science and Catalysis*; Chon, H., Woo, S. H., Park, S. E., Eds.; Elsevier: 1996; Vol. 102, pp 47−74.

(11) (a) Mathews, S.; Ramesh, R.; Venkatesan, T.; Benedetto, J. *Science* **1997**, *276*, 328−240. (b) Mahesh, R.; Mahendiran, R.; Raychaudhuri, A. K.; Rao, C. N. R. *J. Solid State Chem.* **1996**, *122*, 448−450. (c) Wolfman, J.; Simon, Ch.; Hervieu, M.; Maignan, A.; Raveau, B. *J. Solid State Chem.* **1996**, *123*, 413−416.

(12) Bach, S.; Pereira-Ramos, J. P.; Baffier, N. *J. Solid State Chem.* **1995**, *120*, 70−73.

(13) Chen, R.; Zavalij, P.; Whittingham, M. S. *Chem. Mater.* **1996**, *8*, 1275−1280.

(14) Feng, A.; Kanoh, H.; Miyai, Y.; Ooi, K. *Chem. Mater.* **1995**, *7*, 1226−1232.

(15) Brock, S. L.; Duan, N.; Tian, Z. R.; Giraldo, O.; Zhou, H.; Suib, S. L. *Chem. Mater.* **1998**, *10*, 2619−2628.

(16) Suib, S. L.; O'Young, C. L. In *Synthesis of Porous Materials*; Occelli, M. L., Kessler, H. Eds.; Marcel Dekker: New York, 1997; pp 215−231.

(17) Glemser, O.; Gattow, G.; Meisiek, H. *Z. Anorg. Allg. Chem.* **1961**, *309*, 1−19.

(18) Gattow, G.; Glemser, O. *Z. Anorg. Allg. Chem.* **1961**, *309*, 121−150.
(19) Parant, J.; Olazcuaga, R.; Devalette, M.; Fouassier, C.; Hagenmuller, P. *J. Solid State Chem.* **1971**, *3*, 1−11.
(20) Giovanoli, R.; Balmer, B. *Chimia* **1983**, *37*, 424−427.
(21) Golden, D. C.; Chen, C. C.; Dixon, J. B. *Science* **1986**, *231*, 717−719.
(22) Arul Dhas, N.; Koltypin, Y.; Gedanken, A. *Chem. Mater.* **1997**, *9*, 3159−3163.
(23) Lume-Pereira, C.; Baral, S.; Henglein, A.; Janata, E. *J. Phys. Chem.* **1985**, *89*, 5772−5778.
(24) (a) Baral, S.; Lume-Pereira, C.; Janata, E.; Henglein, A. *J. Phys. Chem.* **1985**, *89*, 5779−5783. (b) Baral, S.; Lume-Pereira, C.; Janata, E.; Henglein, A. *J. Phys. Chem.* **1986**, *90*, 6025−6028.
(25) Freeman, F.; Kappos, J. C. *J. Am. Chem. Soc.* **1985**, *107*, 6628−6633.
(26) (a) Ammundsen, B.; Jones, D. J.; Rozière, J.; Burns, G. R. *Chem. Mater.* **1997**, *9*, 3236−3246. (b) Lakshmi, B. B.; Patrissi, C. J.; Martin, C. R. *Chem. Mater.* **1997**, *9*, 2544−2550.
(27) (a) Sostaric, J. Z.; Mulvaney, P.; Grieser, F. *J. Chem. Soc., Faraday Trans.* **1995**, *91*, 2843−2546. (b) Mulvaney, P.; Cooper, R.; Grieser, F.; Meisel, D. *J. Phys. Chem.* **1990**, *94*, 8339−8345.
(28) Antonelli, D. M.; Ying, J. Y. *Angew. Chem., Int. Ed. Engl.* **1996**, *35*, 426−430.
(29) Nazar, L. F.; Koene, B. E.; Britten, J. F. *Chem. Mater.* **1996**, *8*, 327−329.
(30) Tolbert, S. H.; Sieger, P.; Stucky, G. D.; Aubin, S. M. J.; Wu, C.-C.; Hendrickson, D. N. *J. Am. Chem. Soc.* **1997**, *119*, 8652−8661.
(31) Khan, M. I.; Meyer, L. M.; Haushalter, R. C.; Schweitzer, A. L.; Zubieta, J.; Dye, J. L. *Chem. Mater.* **1996**, *8*, 43−53.
(32) Janauer, G. G.; Dobley, A.; Guo, J.; Zavalij, P.; Whittingham, M. S. *Chem. Mater.* **1996**, *8*, 2096−2101.
(33) Chirayil, T.; Zavalij, P. Y.; Whittingham, M. S. *Chem. Mater.* **1998**, *10*, 2629−2640.
(34) Luca, V.; MacLachlan, D. J.; Hook, J. M.; Withers, R. *Chem. Mater.* **1995**, *7*, 2220−2223.
(35) Adams, J. M.; Fowler, J. R. *J. Chem. Soc., Dalton Trans.* **1976**, 201−202.
(36) Bach, S.; Henry, M.; Baffier, N.; Livage, J. *J. Solid State Chem.* **1990**, *88*, 325−333.
(37) Ganguly, P. B.; Dhar, N. R. *J. Phys. Chem.* **1922**, *26*, 701.
(38) (a) Tian, Z.-R.; Tong, W.; Wang, J.-Y.; Duan, N.-G.; Krishnan, V. V.; Suib, S. L. *Science* **1997**, *276*, 926−930. (b) Luo, J.; Suib, S. L. *Chem. Commun.* **1997**, 1031−1032.
(39) Sala, T.; Sargent, M. V. *J. Chem. Soc., Chem. Commun.* **1978**, 253.
(40) *Handbook of Manganese Dioxides Battery Grade*; Glover, D., Schumm, B., Jr., Kozowa, A., Eds.; International Battery Materials Association, 1989; pp 25−32.
(41) Leddy, B. P.; McKervey, M. A.; McSweeney, P. *Tetrahedron Lett.* **1980**, *21*, 2261.
(42) Hildebrand, J. H.; Scott, R. L. *The Solubility of Nonelectrolytes*; Dover: New York, 1964; p 264.
(43) Thiyagarajan, P.; Epperson, J. E.; Crawford, R. K.; Carpenter, J. M.; Klippert, T. E.; Wozniak, D. G. *J. Appl. Crystallogr.* **1997**, *30*, 280−293.
(44) Ressler, T.; Brock, S. L.; Suib, S. L.; Wong, J. *J. Phys. Chem.*, in press,.
(45) Drits, V. A.; Silvester, E.; Gorshkov, A.; Manceau, A. *Am. Mineral.* **1997**, *82*, 946−961.
(46) Wong, S.-T.; Cheng, S. *Inorg. Chem.* **1992**, *31*, 1165−1172.
(47) Post, J. E. In *Biomineralization, Processes of Iron and Manganese, Modern and Ancient Environments*; Skinner, H. C. W., Fitzpatrick, R. W., Eds.; Catena Verlag: Cremlingen-Destedt, 1992; pp 51−73.
(48) Guinier, A.; Fournet, G. *Small-Angle Scattering of X-Rays*; John Wiley & Sons: New York, 1955.
(49) The data were fit using the equation

$$I(Q) = I_0 \int_0^{\pi/2} \left[\frac{2B_1(QR_m \sin\alpha)}{QR_m \sin\alpha} \frac{\sin((QH_m \cos\alpha)/2)}{(QH_m \cos\alpha)/2} \right]^2 \sin\alpha \, \partial\alpha$$

$B_1(x)$ is the first-order Bessel function (Fournet, G. *Bull. Soc. Fr. Mineral. Cristallogr.* **1951**, *74*, 39−113). R_m (cylinder radius), H_m (cylinder height), and a scale factor I_o were obtained (I_o is the same as described previously, as the form factor is normalized; i.e., $I(Q) = I_o P(Q)$ and $P(Q=0) = 1$).
(50) The scattering length density of any material is $\rho_n = dN_a \sum b_i / M_i$ where b_i is the scattering length of the individual atomic components, d is the density (g/cm^3) of the particle due to the structure and individual atomic components, M_i is the atomic weight of each element, and N_a is Avogadro's number.
(51) (a) Herron, N.; Wang, Y. In *Nanomaterials: Synthesis, Properties and Applications*; Edelstein, A. S., Cammarata, R. C., Eds.; Institute of Physics: Philadelphia, 1996; pp 73−88. (b) Stucky, G. D.; MacDougall, J. E. *Science* **1990**, *247*, 669−678. (c) Moller, K.; Bein, T.; Herron, N.; Mahler, W.; Wang, Y. *Inorg. Chem.* **1989**, *28*, 2914−2919. (d) Marinakos, S. M.; Brousseau, L. C., III.; Jones, A.; Feldheim, D. L. *Chem. Mater.* **1998**, *10*, 1214−1219.
(52) (a) Cuy, E. J. *J. Phys. Chem.* **1921**, *25*, 415. (b) Witzemann, E. J. *J. Am. Chem. Soc.* **1915**, *37*, 1079−1091.
(53) Ching, S.; Landrigan, J. A.; Jorgensen, M. L.; Duan, N.; Suib, S. L.; O'Young, C.-L. *Chem. Mater.* **1995**, *7*, 1604−1606.
(54) Ching, S.; Petrovay, D. J.; Jorgensen, M. L.; Suib, S. L. *Inorg. Chem.* **1997**, *36*, 883−890.
(55) Ching, S.; Roark, J. L.; Duan, N.; Suib, S. L. *Chem. Mater.* **1997**, *9*, 750−754.
(56) Duan, N.; Suib, S. L.; O'Young, C.-L. *J. Chem. Soc., Chem. Commun.* **1995**, 1367−1368.
(57) Le Goff, P.; Baffier, N. *Solid State Ionics* **1993**, *61*, 309−315.
(58) (a) Reetz, M. T.; Helbig, W.; Quaiser, S. A.; Stimming, U.; Breuer, N.; Vogel, R. *Science* **1995**, *267*, 367−369. (b) Bönnemann, H.; Brijoux, W.; Brinkmann, R.; Dinjus, E.; Joussen, T.; Korall, B. *Angew. Chem., Int. Ed. Engl.* **1991**, *30*, 1312−1314. (c) Rothe, J.; Hormes, J.; Bönnemann, H.; Brijoux, W.; Siepen, K. *J. Am. Chem. Soc.* **1998**, *120*, 6019−6023.
(59) Fatiadi, A. J. In *Organic Syntheses By Oxidation With Metal Compounds*; Mijs, W. J., de Jonge, C. R. H. I., Eds.; Plenum: New York, 1986; pp 119−260.
(60) Wadsley, A. D. In *Non-Stoichiometric Compounds*; Mandelcorn, L., Ed.; Academic: New York, 1964; p 165.
(61) (a) Chianelli, R. R.; Dines, M. B. *Inorg. Chem.* **1978**, *17*, 2758−2762. (b) Lerf, A.; Schöllhorn, R. *Inorg. Chem.* **1977**, *16*, 2950−2956.
(62) Legendre, J.-J.; Livage, J. *J. Colloid Interface Sci.* **1983**, *94*, 75−83.
(63) Wu, C.-G.; DeGroot, D. C.; Marcy, H. O.; Schindler, J. L.; Kannewurf, C. R.; Liu, Y.-J.; Hirpo, W.; Kanatzidis, M. G. *Chem. Mater.* **1996**, *8*, 1992−2004.
(64) Rebbah, H.; Borel, M. M.; Raveau, B. *Mater. Res. Bull.* **1980**, *15*, 317−321.
(65) Yao, T.; Oka, Y.; Yamamoto, N. *Mater. Res. Bull.* **1992**, *27*, 669−675.
(66) Alberti, G.; Casciola, M.; Costantino, U. *J. Colloid Interface Sci.* **1985**, *107*, 256−263.
(67) Price, S. J.; O'Hare, D.; Francis, R. J.; Fogg, A.; O'Brien, S. *Chem. Commun.* **1996**, 2453−2454.
(68) Treacy, M. M. J.; Rice, S. B.; Jacobson, A. J.; Lewandowski, J. T. *Chem. Mater.* **1990**, *2*, 279−286.
(69) Chirayil, T.; Zavalij, P. Y.; Whittingham, M. S. *J. Mater. Chem.* **1997**, *7*, 2193-2195.
(70) Paterson, E. *Am. Mineral.* **1981**, *66*, 424.
(71) Luo, J.; Suib, S. L. *Chem. Commun.* **1997**, 1031−1032.
(72) Abe, R.; Shinohara, K.; Tanaka, A.; Hara, M.; Kondo, J. N.; Domen, K. *Chem. Mater.* **1998**, *10*, 329−333.
(73) Sasaki, T.; Nakano, S.; Yamauchi, S.; Watanabe, M. *Chem. Mater.* **1997**, *9*, 602−608.
(74) Murphy, D. W.; Hull, G. W., Jr. *J. Chem. Phys.* **1975**, *62*, 973−978.
(75) (a) Mallouk, T. E.; Gavin, J. A. *Acc. Chem. Res.* **1998**, *31*, 209−217. (b) Carrado, K. A.; Xu, L. *Chem. Mater.* **1998**, *10*, 1440−1445.
(76) Le Goff, P.; Baffier, N.; Bach, S.; Pereira-Ramos, J. P. *Mater. Res. Bull.* **1996**, *31*, 63−75.
(77) Dehmlow, E. V.; Slopianka, M.; Heider, J. *Tetrahedron Lett.* **1977**, *27*, 2361−2364.
(78) Giraldo, O.; Brock, S. L.; Suib, S. L. Unpublished results.
(79) Brock, S. L.; Suib, S. L. Unpublished results.
(80) Marcus, Y.; Hefter, G.; Pang, T.-S. *J. Chem. Soc., Faraday Trans.* **1994**, *90*, 1899−1903.
(81) Colic, M.; Fisher, M. L. *Chem. Phys. Lett.* **1998**, *291*, 24−30.
(82) Shimizu, A.; Taniguchi, Y. *Bull. Chem. Soc. Jpn.* **1990**, *63*, 3255−3259.
(83) Holland, K. L.; Walker, J. R. *Clays Clay Miner.* **1996**, *44*, 744−748.
(84) Reynolds, R. C. J. In *Reviews in Mineralogy*; Bish, D. L., Post, J. E., Eds.; Mineralogical Society of America: Washington, DC, 1989; Vol. 20, pp 145−181.
(85) Weller, H. *Angew. Chem., Int. Ed. Engl.* **1993**, *32*, 41−53.
(86) Belal, A. A.; Chaudhuri, P.; Fallis, I.; Farrugia, L. J.; Hartung, R.; Macdonald, N. M.; Nuber, B.; Peacock, R. D.; Weiss, J.; Wieghardt, K. *Inorg. Chem.* **1991**, *30*, 4397−4402.
(87) Chen, J.; Lin, J. C.; Purhoit, V.; Cutlip, M. B.; Suib, S. L. *Catal. Today* **1997**, *33*, 205−214.
(88) (a) Bogush, G. H.; Zukoski, C. F., IV *J. Colloid Interface Sci.* **1991**, *142*, 1−18. (b) Bogush, G. H.; Zukoski, C. F., IV *J. Colloid Interface Sci.* **1991**, *142*, 19−34.